Calibration of the New Horizons Long-Range Reconnaissance Imager

F. Morgan,[a] S.J. Conard,[a] H.A. Weaver,[a] O. Barnouin-Jha,[a] A.F. Cheng,[a] H.W. Taylor,[a] K.A. Cooper,[a] R.H. Barkhouser,[b] R. Boucarut,[c] E.H. Darlington,[a] M.P. Grey,[a] I. Kuznetsov,[c] T.J. Madison,[c] M.A. Quijada,[c] D.J. Sahnow,[b] and J.M. Stock[d]

[a]Johns Hopkins University Applied Physics Laboratory,
11100 Johns Hopkins Road, Laurel, MD, USA;
[b]Johns Hopkins University, Department of Physics and Astronomy,
3400 N. Charles Street, Baltimore, MD, USA;
[c]NASA Goddard Space Flight Center, MS 551, Greenbelt, MD, USA;
[d]Swales Aerospace, 5050 Powder Mill Rd., Beltsville, MD, USA

ABSTRACT

The LOng-Range Reconnaissance Imager (LORRI) is a panchromatic imager for the New Horizons Pluto/Kuiper belt mission. New Horizons is being prepared for launch in January 2006 as the inaugural mission in NASAs New Frontiers program. This paper discusses the calibration and characterization of LORRI.

LORRI consists of a Ritchey-Chrétien telescope and CCD detector. It provides a narrow field of view (0.29°), high resolution (pixel FOV = 5 μrad) image at f/12.6 with a 20.8 cm diameter primary mirror. The image is acquired with a 1024 × 1024 pixel CCD detector (model CCD 47-20 from E2V). LORRI was calibrated in vacuum at three temperatures covering the extremes of its operating range (-100°C to +40°C for various parts of the system) and its predicted nominal temperature in-flight. A high pressure xenon arc lamp, selected for its solar-like spectrum, provided the light source for the calibration. The lamp was fiber-optically coupled into the vacuum chamber and monitored by a calibrated photodiode. Neutral density and bandpass filters controlled source intensity and provided measurements of the wavelength dependence of LORRI's performance. This paper will describe the calibration facility and design, as well as summarize the results on point spread function, flat field, radiometric response, detector noise, and focus stability over the operating temperature range.

LORRI was designed and fabricated by a combined effort of The Johns Hopkins University Applied Physics Laboratory (APL) and SSG Precision Optronics. Calibration was conducted at the Diffraction Grating Evaluation Facility at NASA/Goddard Space Flight Center with additional characterization measurements at APL.

Keywords: Pluto, KBO, space, New Horizons, imager

1. INTRODUCTION

The LOng-Range Reconnaissance Imager (LORRI) is a panchromatic imager for NASA's New Horizons mission to Pluto and the Kuiper belt. The New Horizons spacecraft is currently undergoing testing in preparation for launch in January 2006. The spacecraft is expected to fly by Pluto and its moon Charon between 2015 and 2020, depending on launch date, and then continue outward and fly by a Kuiper belt object (KBO). Since the duration of the Pluto/Charon flyby is much shorter than their rotation periods, only one hemisphere of each body will be visible during close approach. LORRI's primary mission is to provide detailed images of the opposite hemispheres of Pluto and Charon from relatively great distances during approach to and departure from the system. LORRI will also support optical navigation and imaging during the Kuiper belt mission.

All of these applications require a sensitive imager with a small field of view and high resolution. LORRI consists of a Ritchey-Chrétien telescope with a backthinned, back-illuminated 1024 × 1024 pixel CCD detector

Further author information: (Send correspondence to F.M.)
F.M.: E-mail: frank.morgan@jhuapl.edu, Telephone: 1 240 228 8297

at its focal plane (E2V model 47-20). The telescope operates at f/12.6 with a 20.8 cm aperture and 263 cm focal length. The full field of view is 0.29°, and the instantaneous FOV (IFOV) is 5 μrad. The LORRI bandpass extends from approximately 350 nm, where the silicon CCD begins to respond, to a short pass filter cutoff at approximately 900 nm.

This paper discusses the calibration of the LORRI telescope. The calibration facility is described, and an overview of results for point spread function, flat field, radiometric response, detector noise, and focus stability over the operating temperature range is given. Details of the LORRI design, construction and mission are discussed further in the paper by Conard, et al.[1]

The objectives of calibration are most easily understood by reference to the calibration equation, which describes the conversion of the signal observed from a scene in instrumental units to the corresponding value in physical units. In the case of LORRI, the calibration equation can be written

$$I_{x,y,\lambda} = \frac{S_{x,y,\lambda,T,t} - Bias_{x,y,T} - Dark_{x,y,T<t} - Smear_{x,y,\lambda,T,t,\phi} - Stray_{x,y,\lambda,T,t,\Phi}}{FF_{x,y,\lambda,T}\, R_{\lambda,T}\, t}\,, \tag{1}$$

where subscripts x, y denote dependence on detector position (pixel), λ on wavelength, T on temperature, t on exposure time, ϕ on optical power at other points within the FOV, and Φ on total optical power within the telescope. The quantities and their units are I, scene radiance in W m^{-2} sr^{-1} nm^{-1} (see Section 3.5 for an explanation of the spectral units); S, linearized observed signal from scene in DN (for "digital numbers," increments of the digital output from the CCD readout electronics); Bias, the electronic offset of the CCD signal in DN; Dark, the linearized CCD dark current in DN; Smear, the signal in DN acquired by a pixel as it is shifted through a vertical section of the scene during frame transfer; Stray, the signal due to stray light in DN; FF, flat field response, normalizes to the median of a uniform diffuse source; and R, the absolute responsivity in $DNs^{-1}pixel^{-1}/Wm^{-2}sr^{-1}nm^{-1}$. (The units given for radiance and responsivity are for diffuse sources; the solid angle drops out of the corresponding quantities for point sources.) Measurement of the terms of the calibration equation is a primary goal of the calibration. In addition, instrument characteristics such as detector read noise, the imaging point spread function (PSF), and field of view are determined during calibration.

Of the terms in the calibration equation, bias and smear were characterized over the relevant parameters; dark is insignificant at operational temperatures; stray light was tested at discrete off-axis source angles; flat field response has been measured, but there are difficulties obtaining the desired 0.5% accuracy at all pixels from ground-based data, and in-flight measurements are planned to replace or correct the current flat field; and absolute response has been measured with sufficient accuracy for LORRI science goals. The PSF has been measured at several locations across the FOV, and the field of view and read noise have been determined. These evaluations will be described in more detail below.

2. CALIBRATION SETUP

LORRI was calibrated at temperatures spanning its operating temperature range. The telescope assembly temperature ranged approximately from -97°C to -60°C during calibration, while the CCD temperature ranged from -96°C to -78°C. At these low temperatures it was necessary to operate LORRI in vacuum to avoid condensation. The calibration was conducted at the Diffraction Grating Evaluation Facility (DGEF) at Goddard Space Flight Center, which operates a large vacuum chamber where calibrations of several spaceflight optical instruments have been conducted[2].

The LORRI calibration was conducted with four principal objectives: to characterize the flat field precisely for planetary image analysis, to characterize the point source spatial response for KBO observations and optical navigation as well as planetary image analysis, to characterize system parameters such as field of view and detector bias and noise, and to estimate the approximate absolute response for diffuse and point sources for analysis flyby configuration planning. Calibrations were conducted in July 2004 prior to environmental testing (vibration, thermal vacuum, etc.) and again in September after environmental testing to establish stability of the calibration. The post-environmental calibration was more thorough and provided most of the results discussed in this paper. To confirm stability of focus and response over the operational temperature range, key

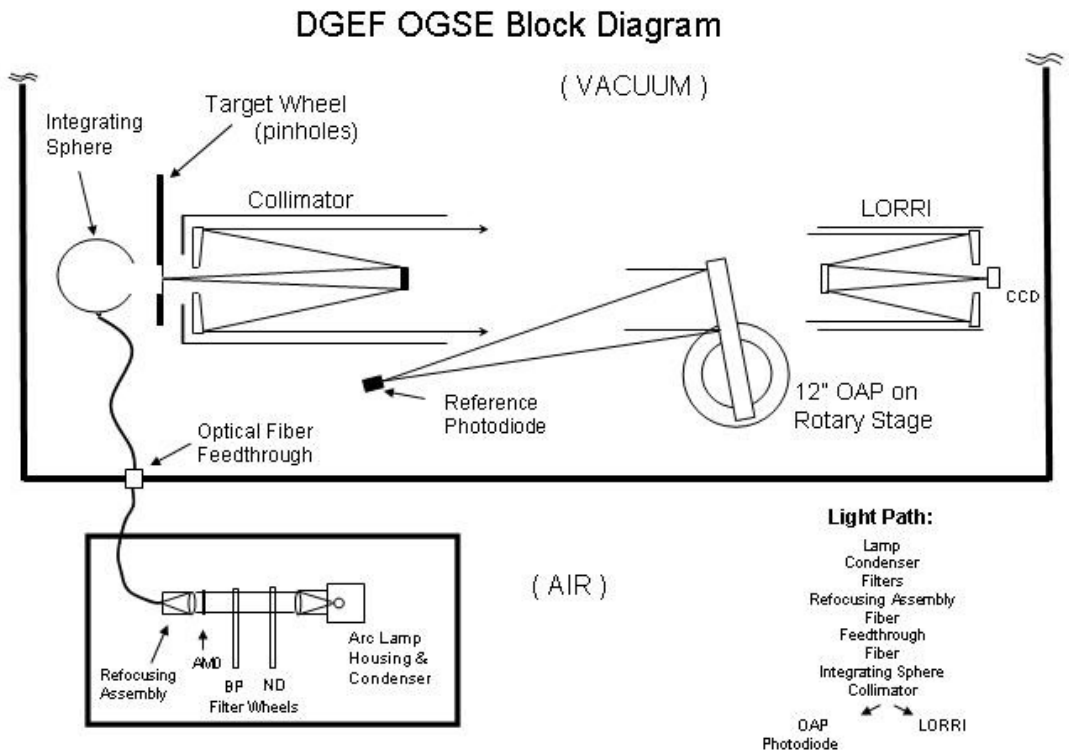

Figure 1. Optical GSE block diagram for the LORRI calibration setup.

measurements were conducted at the nominal temperature as well as temperatures at the upper and lower ends of the operational range.

Figure 1 is a block diagram of the LORRI calibration setup. A light source outside the vacuum chamber was fiber optically coupled into the chamber, feeding an integrating sphere. The integrating sphere backlit a rotating "target wheel" that contained various apertures such as pinholes and resolution targets. The target wheel was at the focal plane of a 38 cm diameter collimator, the output of which illuminated LORRI, which was mounted on a two-axis gimbal approximately two meters from the collimator aperture. Between LORRI and the collimator, a 30.5 cm diameter off-axis parabola could be rotated into the beam to focus a pinhole image onto a calibrated photodiode, providing a measurement of the integrating sphere port radiance for absolute calibration.

The following subsections describe various aspects of the calibration setup in detail.

2.1. Light source

A 150 Watt, high pressure, ozone-free xenon arc lamp was used for the LORRI calibration in order to provide a high radiance, solar-like spectrum. Since there are significant spectral variations in response over the LORRI bandpass, it is important to approximate the expected spectral radiance distribution in order to infer broadband radiometric response from calibration measurements with reasonable accuracy. Sunlight will, of course, provide the illumination for LORRI's imaging in flight. Although the reflectance spectrum of the observed planetary bodies will modify the spectrum, it will remain at least roughly solar-like.

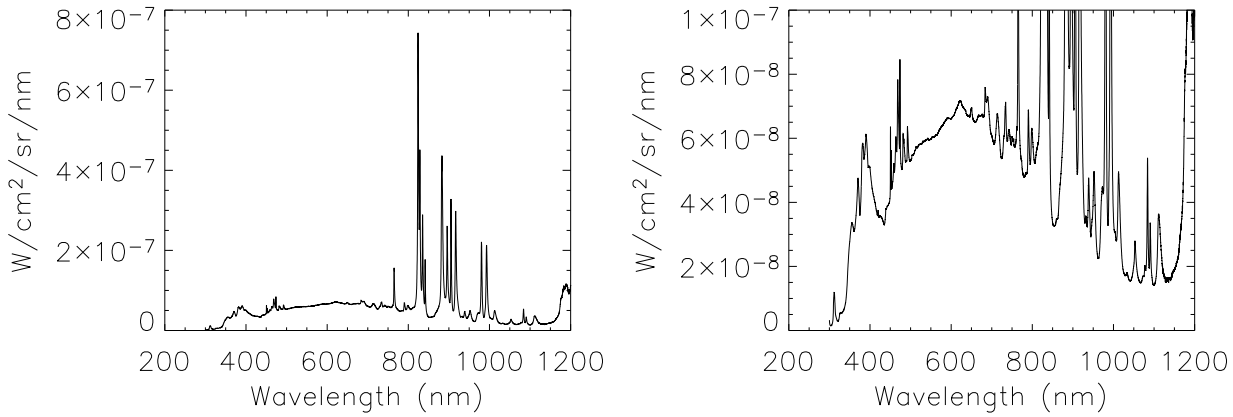

Figure 2. Left: Calibrated flat field source spectrum, taken with ND1 filter and no bandpass filter. Right: Same spectrum shown on a different scale.

The arc lamp output was collimated using a fused silica condenser, transmitted through two six-position filter wheels and an "airmass zero" (AM0) filter, and then focused into a fiber optic using another fused silica condenser. An arc lamp light source was selected in order to couple sufficient optical power into a small optical fiber.

Both filter wheels carried one inch diameter filters. The first filter wheel contained neutral density filters for controlling source intensity. Four filters, with optical densities 1, 2, 3, and 4 were available along with one open (unattenuated) and one opaque position. The opaque position replaced an unused ND5 filter to provide backgrounds.

The second filter wheel contained bandpass filters to test the spectral dependence of LORRI's imaging and response. There were five filters centered at 400 nm, 500 nm, 600 nm, 700 nm, and 850 nm. Bandpasses (FWHM) for the filters were 65 nm for the 400 nm filter, 119 nm for the 850 nm, and approximately 90 nm for the others. Transmission curves were measured with a monochromator prior to the calibration.

A two meter length of optical fiber (Ocean Optics Vis-NIR fused silica, 600 μm core diameter, single strand, NA 0.22) coupled the light source output to a matching vacuum feedthrough (CeramOptec), and then a second two meter length of fiber provided input to an integrating sphere inside the vacuum chamber.

The four inch diameter integrating sphere with a spectralon coating was custom manufactured by LabSphere for vacuum compatibility. It had one SMA fiber input, orthogonal to a 32 mm diameter exit port.

The radiance at the integrating sphere output port, spectrally integrated over the LORRI bandpass, was 46 μW cm^{-2} sr^{-1}. Figure 2 shows the source spectrum. The shape of the spectrum of the integrating sphere input was measured using a monochomator. The monochromator's relative spectral response was determined by scanning a calibrated quartz halogen lamp. Monochromator measurements were made at approximately 0.1 nm resolution to resolve the NIR emission in the arc lamp spectrum. Although the lines appear to dominate the spectrum in Figure 2, they contribute a modest fraction of the total energy in the spectrum because their widths are relatively narrow. The AM0 filter from Spectra-Physics/Oriel (since acquired by Newport) attenuates the NIR portion of the spectrum to make the overall spectral energy distribution more solar-like.

2.2. Collimator and target wheel

Immediately in front of the integrating sphere output port was a "target wheel," a twelve position rotating filter wheel-like mechanism containing various image masks. Key targets included an opaque position, pinholes ranging in size from 5 μm to 1000 μm, a 3 × 3 grid of 5 μm pinholes, an NBS 1963A resolution target, and an open position for flat field measurements. Initially the target wheel opaque position was used for backgrounds

but after experiencing intermittent problems with the target wheel mechanism (which were corrected before post-environmental calibration began), the opaque ND filter wheel position was generally used instead.

The target wheel targets were located at the focal plane of a Cassegrain collimator with a 38 cm aperture, 460 cm focal length, and 0.5° unvignetted field of view. The collimator aperture was large enough to overfill the LORRI aperture without vignetting over the LORRI FOV and gimbal motion range, with tolerance for easy coalignment. The target wheel was positioned to place the 5 μm pinhole (used for point source characterization) at the collimator focus, determined interferometrically using a spherical reflector in the pinhole position.

2.3. LORRI and gimbal

LORRI was mounted on a two-axis gimbal staring back at the collimator approximately two meters away. Looking back through the collimator, LORRI viewed the target wheel image masks effectively at infinity. The gimbal (Aerotech model AOM600M) was stepper motor driven with a Unidex controller at 63 steps per arcsecond to scan LORRI across targets. A LORRI pixel subtends roughly one arcsecond.

2.4. Reference photodiode

Between the collimator and LORRI, a 30.5 cm diameter, 152 cm focal length off-axis parabolic mirror on a motorized rotary motion stage could be sent to one of three positions. A "stow" position swung the mirror fully out of the collimator beam for LORRI observations. A second position focused any of the pinhole targets onto calibrated photodiode for radiometric reference. A third position moved the pinhole image a few millimeters off of the photodiode for photodiode background determination.

The photodiode was a Hamamatsu S1336-8BQ, with a 5.8 mm square active area. Its responsivity was calibrated at Hamamatsu at 10 nm intervals from 200 to 400 nm, and at 20 nm intervals from 400 to 1180 nm. Target pinholes, maximum diameter 1 mm and imaged at 0.33 magnification, were fully captured within the photodiode active area. Photodiode current was brought out of vacuum through a BNC feedthrough and measured with a Keithley electrometer.

2.5. Thermal control

LORRI is passively cooled. To control the telescope temperature during calibration, a shroud surrounding the telescope was liquid nitrogen-cooled. A small annular shroud encircling the telescope inside the cold shroud was heated to control the telescope temperature to the desired setpoint. This method was found to be more stable than controlling the cold shroud temperature directly with controlled cold gas circulation. The thermal conductivity of the telescope structure was sufficient to guarantee a uniform temperature distribution despite the uneven heating. The shrouds were fixed, with LORRI gimbaled inside them. LORRI viewed the collimator through a ten inch aperture in the main cold shroud, which kept the shroud edge well out of the LORRI FOV over the maximum gimbal motion range used. A separate, smaller cold shroud and heater similarly controlled the temperature of the CCD radiator, so the CCD temperature was controlled somewhat independently of the telescope structure temperature. The focal plane electronics board was mounted on the baseplate which supported the LORRI assembly. The baseplate was heated to control the board temperature.

Table 1 lists the temperatures targeted for the nominal, warm, and cold cases, for the CCD, the CCD readout electronics board, and the primary (M1) and secondary (M2) telescope mirrors.

2.6. Command and data

The calibration was controlled by three networked computers. One PC running the Ground Support Equipment Operating System (GSEOS) commanded LORRI, controlling configuration (exposure time and bin mode) and image acquisition. A linux PC hosted a frame grabber to acquire and store LORRI images. A second linux PC acted as the master controller and ran IDL scripts that commanded the calibration GSE mechanisms (gimbal, OAP, target wheel, and filter wheels), cued LORRI commands through the GSEOS PC, and cued LORRI image acquisition through the frame grabber PC.

Table 1. LORRI calibration temperatures (°C).

	Nominal	Cold	Hot
CCD	-80	-93	-75
Board	+26	+10	+35
M1	-72.5	-98.9	-62.1
M2	-73.3	-99.3	-63.5

3. CALIBRATION MEASUREMENTS AND RESULTS

3.1. LORRI operation

Two LORRI configuration parameters, exposure time and bin mode, were important in calibration performance and analysis. The exposure time is the time during which charge accumulates in the CCD under exposure to light before frame transfer and readout. It is electronically controlled; there is no mechanical shutter within LORRI (although for calibration the opaque ND filter wheel position acted as a shutter to block the calibration source). Planned exposure times for the Pluto/Charon flyby are on the order of 50-100 ms and exposure times on this order were used for many measurements. Exposure times up to 967 ms were used frequently in measurements when the source was relatively weak, for example, when viewing the 5 μm pinhole, or any target in combination with the 400 nm bandpass filter. Exposure times up to several seconds were employed for linearity tests.

The bin mode controls on-chip summing of signal in multiple pixels during CCD readout, and was selectable between 1×1 (all pixels read out individually, producing a 1024×1024 image) and 4×4 (pixels summed in blocks of 16 pixels, producing a 256×256 image). The primary purpose of the 4×4 bin mode is to increase sensitivity for long range KBO detection and navigation imagery. For flyby imagery, 1×1 bin mode will be used for high resolution. Measurements intended to characterize terms in the calibration equation were conducted in both modes. The following discussion concentrates on 1×1 bin mode measurements, since they are expected to apply for the imagery of greatest scientific interest.

3.2. Detector bias and read noise

The detector read noise was estimated from zero exposure time exposures taken in the DGEF at nominal temperature with no illumination. One hundred images were acquired, and the standard deviation of the signal of each pixel was evaluated. The distribution of the standard deviations is plotted in Figure 3. The most probable standard deviation is 1.2 DN, which is adopted as a read noise estimate. Similar results have been obtained in subsystem level detector tests.

The detector bias (signal at zero illumination due to electronic offset) depends on the focal plane electronics board temperature. From subsystem level tests, the relationship $504.6 + 1.22T$ has been found to estimate the bias in DN as a function of board temperature T in °C. The expected flight board temperature range is +30°C to +50°C. The bias ranges from 541 to 566 DN over that range.

Detector dark current is negligible over the flight CCD temperature range, for exposure times up to at least one second. Planned exposure times are on the order of 100 ms.

3.3. Point source imaging

During calibration at the DGEF, point source imaging performance was evaluated by observing a 3×3 grid of 5 μm pinholes. The grid target was arranged with 4 pinholes near the corners of the FOV, 4 along the edges, and one near FOV center. LORRI was gimballed through a 6×6 subpixel grid of positions spanning approximately 1.5 pixels, acquiring 10 images at each step. A fitting process was applied to the images to estimate the subpixel irradiance distribution. Results indicated a FWHM on order of 2 pixels, with no discernible dependence on position within the FOV. No significant variation of the FWHM with temperature was observed, verifying focus

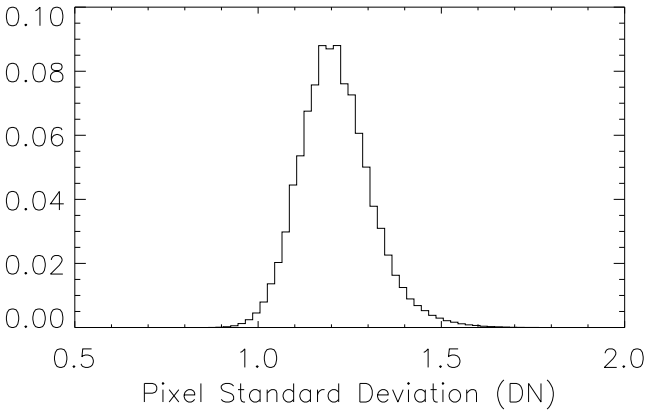

Figure 3. Read noise distribution. Standard deviation of each pixel calculated over a series of 100 unilluminated, zero exposure time images. The signal and its standard deviation are in units of "DN" (digital numbers), the digitized output of the CCD readout. The histogram plots the fraction of pixels with standard deviations in 0.02 DN wide bins at the values plotted along the x-axis.

stability over the temperature range from ambient to -100°C. These tests were adversely affected by diffraction by the collimator secondary obscuration, which was larger than the LORRI secondary.

More accurate PSF measurements were obtained in bench tests at ambient temperature at APL. A source was projected through a Laser Unequal Pathlength Interferometer (LUPI) and then an off-axis parabola collimator with an unobstructed aperture to generate a collimated beam that filled LORRI's aperture completely. Collimator focus and alignment was verified by reflecting the beam back into the LUPI from an optical flat at the collimator output. For LORRI tests the beam was reflected from an optical flat mounted with tip/tilt controls, which allowed focus and PSF measurement at five positions in the LORRI FOV (near the corners and near the center). Image analysis indicated a PSF FWHM of 1.5 pixels with little variation across the FOV, when fit with a two dimensional Gaussian function. With the spot near pixel center, ensquared energy in a pixel exceeded 0.3 at all four corners and the center of the CCD.

3.4. Flat field

The initial LORRI flat field was derived from measurements during the post-environmental calibration at the DGEF observing the open target wheel position, which filled the LORRI FOV except for small areas in the corners. These areas were covered with additional images taken after gimballing LORRI 0.15° to the left and right. Flat field variations are small with over 97% of the pixels within ±2% of the median. Several small areas were shadowed by dust particles which apparently fell onto the CCD and the field flattening lenses during vibration testing. Approximately 152 pixels were affected by these particles at the time of the post-environmental calibration. The CCD was subsequently cleaned by blowing ionized nitrogen across it. New flat field measurements conducted at APL showed that the number of pixels affected by particle shadowing was reduced to 62. However, these new flat field measurements were conducted in air at room temperature, conditions differing significantly from flight. In addition, the light source was an incandescent lamp with a significantly non-solar spectrum. No flat field data obtained thus far applies perfectly to the flight system. We plan to obtain flat field data in flight, possibly during the Jupiter flyby, either to use directly or to patch the DGEF flat field where particle shadowing effects have changed.

Further discussion of the DGEF flat fields is warranted by the fact that, apart from the particle effects, the DGEF flat fields characterize the system flat field performance and demonstrate flat field stability over the operating temperature range. For the panchromatic flat field (bandpass filter wheel open, ND 1), 100 flat field images were acquired at each azimuth angle (0 and ±0.15°). 100 background images with the light source blocked

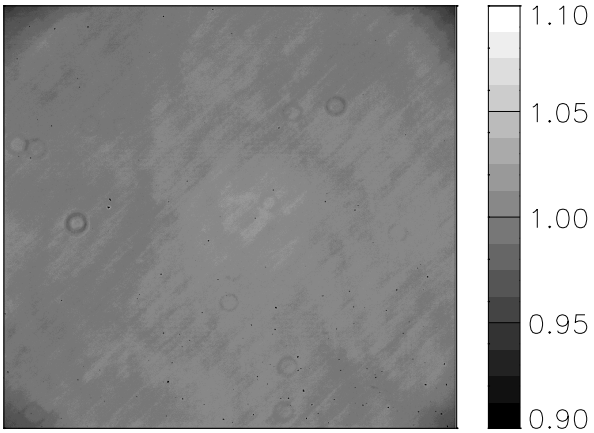

Figure 4. LORRI flat field variation from DGEF calibration. Range scaled to exaggerate structure. See discussion in Section 3.4.

at the ND filter wheel were obtained for each observation and subtracted from the flat field images, and the background subtracted images were averaged. Similar flat field data was acquired for each bandpass filter, but the ND filter was open and only 10 images were taken. A composite flat image was created by stitching the center, left and right images together. The composite image consists primarily of the center image, with pixels more than 545 pixels from the center replaced by scaled signal from the left and right images. The off-axis images were scaled by the ratio of the medians of signal in pixels along the border between the center and corner regions. For the panchromatic flat fields at nominal temperature, the scale factors were 1.0066 and 1.0045 for the left and right corners, respectively; the intensity variation was small and consistent with the variation in reference photodiode current. For the bandpass filtered flat fields, scale factors ranged from 0.990 to 1.021.

The composite flat field image was divided by its median to obtain the relative flat field variation, which is shown in Figure 4 for the flat field derived from the nominal temperature case. Vignetting of approximately 4% is seen in the corners, consistent with expectations based on the design of the baffles and stop. Small, dark "doughnut" like rings are probably out of focus shadows from particles on the field flattening lenses. Small, dark spots are particles directly on the CCD. A central region of approximately 200 pixel radius is brightened approximately 0.5% by a ghost that results from multiple reflections between surfaces within the field flattening lens group. The ghost depends somewhat on source spectrum and on the radiance distribution over field angles beyond the FOV up to approximately 0.3° off axis.

The flat field showed no significant temperature dependence. The maximum differences between the flat field at nominal temperature and those at the hot and cold extremes were on the order of 1%, with fewer than 250 pixels exceeding 0.5% variation in either case. Bandpass filtered flat fields showed somewhat more variation with temperature, but for most of the filters the variations are not statistically significant. Only 10 images were used for the filtered flats, compared to 100 for the panchromatic flats. There appeared to be significant temperature dependence in the 850 nm flat, possibly due to etaloning in the CCD interacting with the emission lines in the xenon arc lamp spectrum. These strong lines would not occur in natural targets, and the polychromatic results indicate that these effects are strongly diluted in unfiltered light. The flat field is practically independent of temperature for flight conditions.

3.5. Absolute response

The absolute response of a panchromatic system is fundamentally difficult to define. When responsivity varies significantly over the bandpass the signal depends on the scene spectrum, which will vary somewhat across different planetary terrains. There will always be some ambiguity in radiometric interpretation of panchromatic imagery when the scene spectrum is unknown. For that reason, LORRI is not intended to provide precise radiometry. However, the source spectra that LORRI will view in flight will be constrained somewhat by the

fixed spectrum of the illuminating source (the sun), modified by variable surface albedos. LORRI may provide some useful radiometric data as long as the range of uncertainty due to unknown source spectrum can be estimated. It is also important for observation planning to establish the approximate absolute response, so that exposure times can be set to provide reasonable signals, for example.

In order to determine the dependence of LORRI response on scene spectrum, it was necessary to estimate LORRI's absolute responsivity as a function of wavelength. This was done using panchromatic absolute measurements together with a calculated relative response curve. First, the LORRI responsivity spectrum was calculated from geometrical throughput considerations and estimates of subsystem spectral performance. It was assumed that this curve approximated the shape of the LORRI response spectrum, and that an unknown constant factor would scale it to the correct absolute level. Second, the LORRI response spectrum was determined using

$$R_{\lambda,T} = \rho_\lambda \left[\frac{S_T \left(D_L^2 - B_L^2 \right)}{(D_L^2 - B_C^2) \int I_\lambda(\lambda) \rho_\lambda(\lambda) d\lambda} \right], \tag{2}$$

where D_L is the LORRI aperture diameter, B_L and B_C are the effective obscuration diameters of the secondary and spider of LORRI and the collimator, respectively, S_T is the LORRI calibration signal at temperature after flat field correction, I_λ is the calibrated source spectral radiance (Figure 2), and ρ_λ is the calculated LORRI response curve. The quantity in square brackets scales the calculated relative response curve ρ_λ to the absolute response required to fit the observed calibration signal S. The ratio of geometric terms corrects for signal reduction from the partial blockage of LORRI's aperture by the collimator secondary, which is larger than LORRI's secondary. Lastly, the response to a range of realistic scene spectra was calculated numerically by integrating the product of the assumed scene spectra and the LORRI response spectrum derived from calibration. Bandpass filter response measurements confirm that the shape of the main portion of the LORRI response spectrum is reasonably approximated by the calculated curve. These steps are described more fully as follows.

The a priori LORRI responsivity spectrum calculation included mirror size and secondary obscuration (11%), the measured curves for reflectance of the two mirrors and transmission of the lenses, and E2V's typical quantum efficiency curve for the model 47-20 CCD. The curve is shown in Figure 5 (after scaling to fit the observed calibration signal). For comparison, points are shown representing monochromatic response inferred from bandpass filter measurements. These results will be discussed below.

The same observations from which the flat field was derived were used to estimate LORRI response. The flat field source spectrum was determined as described in Section 2.1, and corrected to an absolute scale using reference photodiode measurements taken immediately after each set of flat field images. The 1 mm pinhole was imaged onto the calibrated photodiode with the OAP mirror. Knowing the shape of the spectrum (after correcting for the measured OAP reflectance), the photodiode current indicates the power emitted through the pinhole and collected by the OAP. Dividing by the pinhole area and the solid angle of the OAP (less the obscuration by the collimator secondary) yields the spectral radiance of the integrating sphere port, shown above in Figure 2 at the level determined during the panchromatic, nominal temperature flat field measurements.

The LORRI signal was taken from the median flat field signal, which was the normalization for the flat field derivation discussed in Section 3.4. For polychromatic flat fields both LORRI images and photodiode measurements were made with the ND1 neutral density filter in the beam, so no explicit correction is required. Accounting for the 80 ms exposure time, the LORRI signal was 15908 DN/s/pixel viewing the diffuse source spectrum shown in Figure 2. From this signal, the absolute LORRI response curve shown in Figure 5 is derived from Equation 2. The resulting curve is 14% below the nominal calculated response curve.

From the calibrated response curve, LORRI's responsivity to various realistic scene spectra can be calculated by integrating the product of the LORRI absolute response and the normalized scene spectrum, where the scene spectrum is normalized to unity in the units in which radiometric estimates would be reported. We plan to report radiance in terms of the spectral radiance at the LORRI pivot wavelength,[3] 607.6 nm. LORRI does not directly measure spectral radiance at any wavelength, since it is sensitive to the integrated spectrum over its relatively wide bandpass. However, given an adopted relative spectrum, reporting the spectral radiance at a specified (though more or less arbitrary) wavelength is a convenient way to specify the absolute level of the overall spectrum. Given this approach for reporting LORRI radiometric results, the responsivity can then be

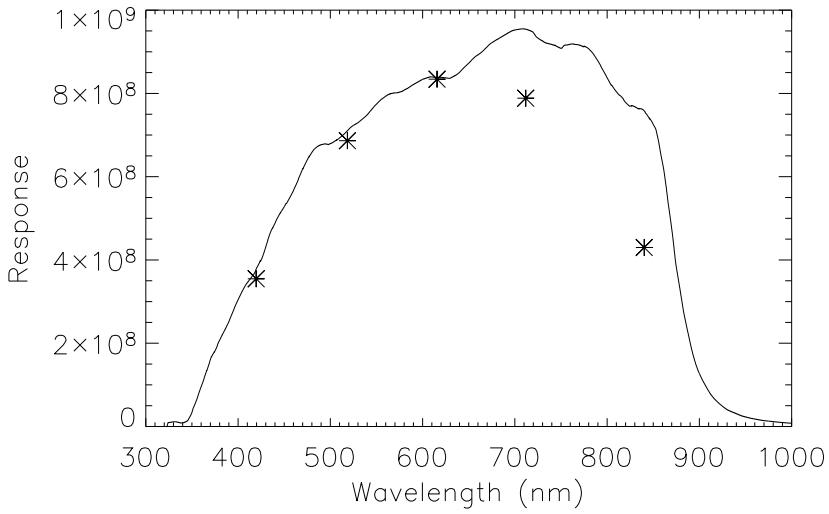

Figure 5. Calibrated LORRI responsivity spectrum, (DN/s/pixel)/(W/cm^2/sr). Asterisks mark monochromatic response points derived from bandpass filter measurements.

expressed in units of (DN/pixel/s)/(W/cm^2/sr/nm). The spectral radiance in the denominator is understood to correspond to the pivot wavelength. The response depends on the shape of the adopted scene spectrum, and has been calculated for three spectra covering the range of spectra we expect to encounter with planetary and KBO observations. The globally integrated spectrum of Pluto, derived from ground-based measurements, defines an intermediate representative spectrum that is probably typical of average Pluto terrains. Isolated areas the surfaces of Pluto, Charon, and KBO's may range from more or less white frost-covered surfaces to terrains as red as asteroid 5145 Pholus (W. Grundy, personal communication, 2004). Corresponding spectra are shown in Figure 6, and LORRI responsivities to each spectrum are given in Table 2. The 20% range between response extremes suggests the range of uncertainty introduced by ignorance of the true scene spectrum.

Table 2. LORRI diffuse source responsivity for typical and extreme spectra.

Spectrum	Responsivity (DN/s/pixel) / (W/cm^2/sr/nm)
Solar (frost)	2.957×10^{11}
Pluto (global)	2.186×10^{11}
5145 Pholus	3.406×10^{11}

As an example, suppose LORRI measures a signal of 1500 DN with a 100 ms exposure from a relatively bright area on Pluto's surface. Suspecting the bright area might be a relatively white, frost-covered terrain, we assume that the spectrum is close to solar. Dividing the 1.5×10^4 DN/s/pixel signal by the 2.96×10^{11} solar response (Table 2) indicates that the spectral radiance is roughly 50 nW/cm^2/sr/nm at 607.6 nm. Given solar spectral irradiance approximately 160 nW/cm2/nm at that wavelength at Pluto's distance, the hypothetical observed radiance is similar to a white Lambertian surface illuminated at normal incidence.

Estimates of monochromatic response at bandpass filter wavelengths confirm the assumption that the calculated response spectrum reflects the shape of the true response curve at wavelengths shorter than 700 nm. At 700 nm the calculated curve is 17% above the measured value. The discrepancy may reflect an underestimate of the CCD quantum efficiency at that wavelength. Since wavelengths longer than 650 nm contribute about

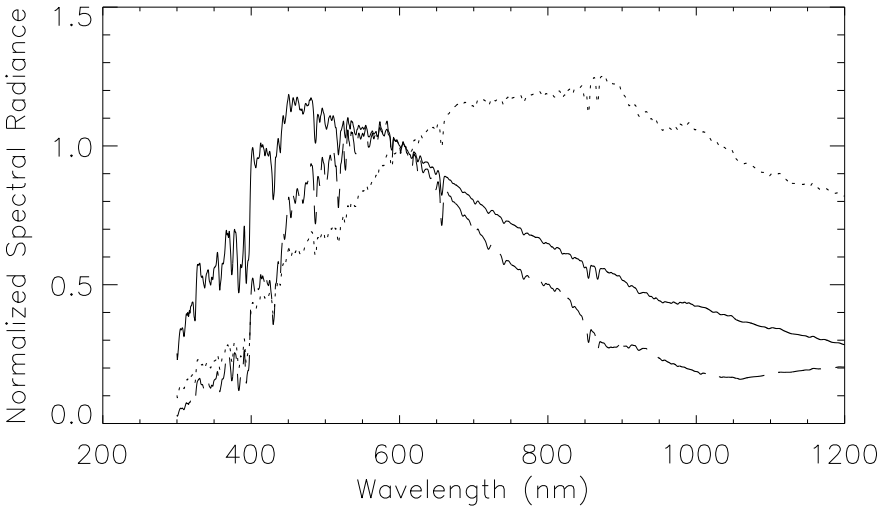

Figure 6. Spectral radiance of white surface (solid line, solar spectrum), average Pluto (dashed), and asteroid 5145 Pholus (dotted). All spectra normalized to unity at 607.6 nm, and smoothed to 3 nm resolution for greater graphical clarity.

40% of LORRI's signal, the 17% uncertainty in response at 700 nm would have less than a 7% effect on total response, which is not significant compared to the 20% uncertainty that can be expected given uncertainty in source spectrum. A more severe difference of 43% at 850 nm is probably related to the difficulty of interpreting a relatively broad bandpass (119 nm) measurement in a region where the response is changing sharply, possibly in addition to complications from the xenon emission lines. The bandpass filter data confirm that the assumed relative LORRI response curve is adequate for radiometric analysis at the limited level intended for LORRI imagery. In-flight observations of G-type standard stars might be used to confirm the LORRI absolute response to solar-like spectra.

Absolute response to point sources was estimated from the diffuse source response result. Given the 2.4×10^{-11} sr solid angle subtended by a LORRI pixel, the 2.957×10^{11} (DN/s/pixel)/(W/cm^2/sr/nm) diffuse source responsivity becomes approximately 1.2×10^{22} (DN/s/pixel)/(W/cm^2/nm) response to a point source with a solar-like spectrum. At a 100 ms exposure time, and capturing approximately one third of the total signal in the peak pixel, LORRI will achieve a SNR of approximately 27 observing a magnitude 11.5 star. This more than satisfies the sensitivity requirements (SNR > 7) for opnav and KBO detection. This rough estimate of point source response suffices for establishing that sensitivity requirements are met. However, much improved point source response measurements will be made by observing standard stars during the flight to Pluto.

3.6. Field of view

The LORRI field of view was determined from a series of images viewing the 5 μm pinhole. Images were acquired at a series of gimbal steps that crossed each edge of the detector at three positions along the edge. Steps were separated by approximately 12 pixels. Images for each gimbal position were averaged and centroided to determine the image position. The gimbal position at the edge of the detector was interpolated from the gimbal angles and image positions of the two images closest to the edge for each series. The field of view was estimated from the difference between gimbal angles at opposite detector edges. Fields of view across field center are 0.2930° horizontal $\times$ 0.2917° vertical. For transects closer to the edge of field (for example, the horizontal FOV near the top edge of the CCD), the FOV is typically approximately 0.5 arcseconds smaller than the corresponding transect near FOV center. This may indicate very slight pincushion distortion. A separate calibration was carried out to map distortion across the FOV, but has not yet been analyzed.

4. CONCLUSION

Calibration measurements have characterized LORRI's detector parameters, and flat field and point source performance have been verified. Radiometric response to diffuse and point sources has been estimated; radiometric interpretation of panchromatic imagery is always ambiguous when scene spectra are unknown, but the response has been calculated for a realistic range of scene spectra and useful radiometric information will be derivable from LORRI data despite the modest ambiguity. The flat field results may be corrected or replaced in flight due to difficulties establishing accuracy at the desired 0.5% level over limited regions of the FOV, because of the ghost and the particulate contamination. Also, although point source imaging performance has been verified to remain stable over temperature, accurate determination of the PSF awaits in-flight stellar observations. Overall, the instrument is well understood and ready to provide unprecedented imagery at Pluto and Charon and the Kuiper belt.

ACKNOWLEDGMENTS

The LORRI calibration team would like to acknowledge Lana Pryde of Newport/SpectraPhysics/Oriel for helpful advice on selection of arc lamp light source components, and Brian Lai and Ken Ashton of Labsphere for engineering the integrating sphere. LORRI calibration was funded under NASA contract NAS 5-97271.

REFERENCES

1. S. Conard, F. Azad, J. Boldt, A. Cheng, K. Cooper, E. Darlington, , M. Grey, J. Hayes, P. Hogue, K. Kosakowski, T. Magee, M. Morgan, E. Rossano, D. Sampath, C. Schlemm, and H. Weaver, "Design and fabrication of the New Horizons Long-Range Reconnaissance Imager," in *Astrobiology and Planetary Missions*, G. R. Gladstone, ed., *Proc. SPIE* **5906**, 2005.
2. M. Quijada, J. Stock, R. Boucarut, T. Saha, T. Madison, and T. Zukowski, "Optical stimulus for the calibration of the ultraviolet and optical telescope (uvot) for swift," in *X-Ray and Gamma-Ray Instrumentation for Astronomy XIII*, K. Flanagan and O. Siegmund, eds., *Proc. SPIE* **5165**, 2004.
3. K. Horne, *The ways of our errors: optimal data analysis for beginners and experts*, star-www.st-and.ac.uk/ kdh1/pub0/ada/woe/woe.ps, University of St. Andrews, 2004.